Morphologically driven swimming dynamics of the longnose skate

Alex Kaplan[1], Megan Vandenberg[2, 3,] John Michael Racy[4], Adam Summers [2, 3], Ed Habtour[4], Bart Boom[4]

REU-Blinks Program 2025
Summer 2025

[1] University of California Santa Cruz, MCD Biology, Santa Cruz CA 95064
[2]University of Washington, Department of Biology, Seattle WA 98195
[3]Friday Harbor Laboratories, Friday Harbor WA 98250
[4]University of Washington, College of Engineering, Seattle WA 98195

Contact Information:
Alexandria Kaplan
Molecular, Cellular, and Developmental Biology Department
1156 High St
Santa Cruz CA 95064
ark.fishing@icloud.com

Keywords: Skate, *Raja rhina*, swimming, biomechanics, morphology, elasmobranch

Abstract:

Skates propel themselves using winglike pectoral fins that generate undulatory waves along the body. We hypothesize that their skeletal morphology, parallel rows of fin rays composed of mineralized radials, enhances locomotion by passively directing waves through stiffness. Stiffness decreases distally down each fin ray due to bifurcation, and the space between parallel fin rays reduces stiffness along the anterior to posterior axis of the fin. We compared swimming in a live longnose skate (*Raja rhina)* to the passive motion of a deceased specimen driven by a vertical linear actuator. We used motion tracking to quantify frequency, wavenumber, and amplitude. We investigated whether an undulatory wave can be passively generated without muscle activation, and at what frequencies it most closely resembled live swimming. We observed that for live swimming, small increases in frequency were able to significantly increase swimming velocity, with the skate having a preferred frequency and wavenumber range. This range also matched the observed values calculated from the dead skate's response, with similar frequencies of maximum amplitude for the live and deceased skate. At these peak frequencies, the output wavenumbers also matched. These results indicated that morphology alone supports wave propagation without active muscle input. Musculoskeletal structure constrains and optimizes the swimming frequency and wavenumber, highlighting the role of passive mechanics in undulatory swimming in the longnose skate.

Introduction:

Batoids fishes have evolved specially adapted wing-like pectoral fins that allow them to generate thrust, lift, yaw, and roll through a variety of swimming styles (Bottom II et al., 2016; Jeong & Lee, 2024; Rosenberger, 2001). Batoids are a subdivision of chondrichthyes, or cartilaginous fishes, descending from ancestral sharks, all falling under the elasmobranch suborder. Commonly referred to as skates and rays, these fishes are distinct by their flattened bodies and dorsoventrally compressed pectoral fins that span most of their body trunk.

There are over 550 known batoid species around the world, with over 200 of those species being recognized under the family Rajidae, or skates. Skates primarily inhabit the benthos, with no recorded pelagic species (Ebert & Compagno, 2007). On the sea floor, they locomote using only their pelvic fins by punting off the seafloor (Koester & Spirito, 2003 & observational). Use of their pectoral fins is generally reserved for quick movements, or when the skate rises off of the floor (observational). Variance in batoid wing morphology can be attributed to environmental and locomotive drivers (López-Romero et al., 2025). Variation in pectoral shape is significant to the evolution of different swimming models, with skates specifically adapting their fins to support fine-scale maneuverability (Martinez et al., 2016). Additionally, the fins have non-uniform stiffness based on the calcification of the cartilaginous skeleton, which is laterally correlated with the fin’s bending (Schaefer & Summers, 2005). Cartilaginous fishes lack swim bladders making them negatively buoyant, with skates living as benthic species (Bone & Roberts, 1969). This means they need to generate their own lift through swimming mechanics (Rosenberger, 2001).

Rosenberger described a range of different movement patterns within batoids in two broad categories; undulation and oscillation. These categories are defined by the moving wave that is propagated down the fish's fin when swimming. Oscillatory fishes move through the water in a flapping motion with less than one wave along the fin, whereas undullatory fishes pass more than one wave down their fin structures with a wavenumber greater than 1.0 (Rosenberger, 2001). This makes undulatory fishes effective at slow swimming, because they are able to generate most of their propulsion through the added mass effects, where fluid is accelerated at the posterior of the body allowing for more consistent thrust production (Bottom II et al., 2016). Skates often fall in the middle of this continuum as intermediate undulators with a wavenumber of around 1.1 (Martinez et al., 2016; Rosenberger, 2001, observed). Looking at the swimming mechanics of other undulators, the blue-spot stingray, *Taeniura lymma* (average wavenumber 1.4)*,* only activates its anterior muscles of the fin at low speeds, with the posterior muscle remaining passive (Rosenberger, 2001; Rosenberger & Westneat, 1999). This brings into question how much of a batoid's locomotion is generated passively by their morphology.

Batoid cartilaginous skeletons consist of an inner pterygial complex with hundreds of fin rays extending out to form the pectoral fins. Each ray consists of tens of radials, which bifurcate distally from the complex (Schaefer & Summers, 2005). Batoid cartilaginous skeleton elements vary between undulatory and oscillatory batoids. Longnose skates are undulatory swimmers with a wavenumber of around 1.1 (observed).

Schaefer and Summers (2005) describe how *rajadae* fish have a catenated calcification, where the mineralization forms 2-4 spokes down each radial (Huang et al., 2017). This morphology allows for a lighter skeleton which is energetically cheaper to build and move. There is also a lateral stiffness gradient with the proximal and medial catenated radials being more stiff, and the thinner post-bifurcated distal radials being less stiff (fig. 6) (Schaefer & Summers, 2005). Decreased stiffness gives the wing tip greater flexibility suggesting amplification of spanwise impulses traveling from the stiffer basal region.

A mechanism for making a deceased fish swim has been modeled in rainbow trout (*Oncorhynchus mykiss*) where Beal et al. used a vertically mounted half cylinder to shed vortexes in a water column to see if the dead fish would still "slalom" between them (Beal et al., 2006). Live fish had previously been discovered to move their bodies between the shedding of vortices in a fashion allowing them to propel forward. The fish beat its tail in the rhythm of the vortical shedding to catch the propulsive ends, allowing the fish to swim upstream (Liao et al., 2003, 2003). This was also seen in saithe fish where the fish adjusted its muscle tension to generate body resonance frequencies to maximize the tail's oscillations (Kohannim & Iwasaki, 2014). A resonant frequency (Ω = sqrt(k/m)) is when a certain input frequency produces an output amplification in a system. Bass are able to decrease their energy expenditure by adjusting their body stiffness (k) to be in resonance with the frequency they beat their tail at (Long & Nipper, 1996). Beal et al. showed how dead fish can also follow between vortices at the right frequency meaning that in ideal conditions, the swimming motion can be passive. This study suggested that due to streamlining of the body, a side-to-side passive oscillation is generated, which is able to extract energy from the vortexes (Beal et al., 2006). The batoids we are considering are different from these carangiforme fishes in that they do not use their tail to swim. We demonstrated that batoids can similarly generate passive anteroposterior traveling waves as an attribute to their own morphology.

Studying the passive generation of movement for batoids is relevant for the engineering of biologically informed robots. Current batoid-inspired builds have implemented different approaches such as using multiple sequentially activated motors to produce a wave (Yang et al., 2009). This model suppresses the design's ability to model natural batoid waves by artificially forcing waves to propagate. Jeong et al. (2024) used an oscillatory model to show that when motion input is restricted to the leading edge, the model was able to generate greater oscillations down the rest of the fin (Jeong & Lee, 2024). This supports the hypothesis on passive morphology, a wave is propagated down the entire fin even when the input is restricted. There are also single actuator compliant robotic designs that leverage this by increasing degrees of freedom (Valdivia y Alvarado, 2011). This allows for the fin to elastically interact with the vortices. These vortexes include the leading edge vortex (LEV) which propagates to form edge vortexes. The LEV creates a dorsoventral pressure differential, which is the mechanism behind lift (Bottom II et al., 2016). This model uses a stiffer polymer for the anterior half or the fin and a softer polymer for the posterior, with no skeleton. This binary solution does not accurately replicate the soft tissue morphology, with no skeleton to utilize the use of internal structure to define more intricate stiffness gradients. While current robotic batoid models have machinery that generate waves, our goal is to show the creation of these waves relates to the form and function of the internal batoid wing structure.

We will explore the difference in response between a living and deceased skate by testing different ranges of frequencies to see both when we get a greater response as well as how this compares to live batoid swimming. 1) By exploring response in gain (output over input) we will analyse how the model responds across a range of frequencies to determine when the system is amplified. 2) We considered the output wavenumber of the skate to determine if undulatory patterns are also functions of morphology. 3) By comparing the swimming of a living versus deceased skate, we are keeping the morphological form of our fish the same in order to determine what aspects of swimming can be attributed to morphology. This study applies interdisciplinary aspects of engineering structural vibrations and biomechanics to explore how evolved dynamic passivity can inform more efficient batoid-informed designs.

Methods:

Specimen Collection and Handling:

We collected one *Raja rhina* (Longnose skate) on a bottom-trawl in the San Juan channel under IACUC protocol #4238-03. The longnose skate specimen has a total length (tip of nose to the cartilaginous tip of the tail) of 184.82 mm, disc width (tip of each pectoral fin) of 118.4 mm, and a disc length (tip of nose to base of tail) of 87.8 mm. This size was ideal for the experiment because the skate swam in the middle of the flume without experiencing any wall effects (Webb, 1993). For the duration of the live behavior trials, the skate was kept in flow-through housing and fed fresh shrimp caught off the coast of the San Juan islands three times a week. When filming, the skate was placed in the flume during active filming and was able to rest between trails in a separate aerated sea-water tank. Trials lasted for around 15 seconds, concluding when the skate started to swim to the surface. When the skate showed signs of fatigue, filming was halted to allow the skate from a few minutes to a few hours of rest. The specimen was euthanized with a lethal dose of MS-222 (Tricaine mesylate) after testing.

Behavioral Filming:

The skate was filmed using a Fastex imaging camera (HS7) and M. Zuiko Digital lens (ED 12-40 mm F2.8 PRO II) at 78 frames s^{-1} . The skate was placed in a 152.4 × 38.1 × 50.8 cm flume tank (Rolling Hills Research Corporation, Model 1520 Water Tunnel) that was filled with fresh sea water. The flume allowed for laminar flow where the skate swam at varying flow speeds of; 65.53, 72.14, 87.38, and 96.52 mm/s (or in body lengths; 0.75, 0.82, 0.99, and 1.10 body length per second, with body length defined as disc length). The camera was placed perpendicular to the flume with water flowing left to right across the camera frame. The flume was illuminated from the bottom and top of the tank (Fig. 1a). The skate was gently released into the middle of the flume where its swimming behavior was measured. The initial movements when the skate was released into the tank were not included in the data analysis to account for non-steady swimming. A total of seven videos were used for data analysis, two videos at 0.75, 0.82, and 0.99 body lengths per second, and one video at 1.10 body lengths per second.

Actuation Experiments:

After the skate was euthanized, it was attached to an actuator where a sine input motion was generated. The skate was mounted through the cartilaginous spine between its gills and posterior of its eyes, using a screw with two washers on the dorsal and ventral side to evenly distribute the input force. The skate was then filmed oscillating at a constant amplitude of 20 mm at varying frequencies from 1.8 to 2.5 Hz with step-ups of 0.1 Hz. Fastex imaging cameras (HS7) with M. Zuiko Digital lens (ED 12-40 mm F2.8 PRO II) filmed at 200 frames s-^{1} from the sides and bottom (Fig. 1b). The skate was oscillated at each frequency for 10 full cycles with a few oscillations at the beginning and end to calm the transition to the next frequency. Between each frequency, the system waited for five seconds before beginning the next test, where frequencies increased in 0.1 Hz increments. Filming occurred within 90 minutes post-mortem to avoid major effects of rigor mortis. There was no flow present during the deceased skate experiments.

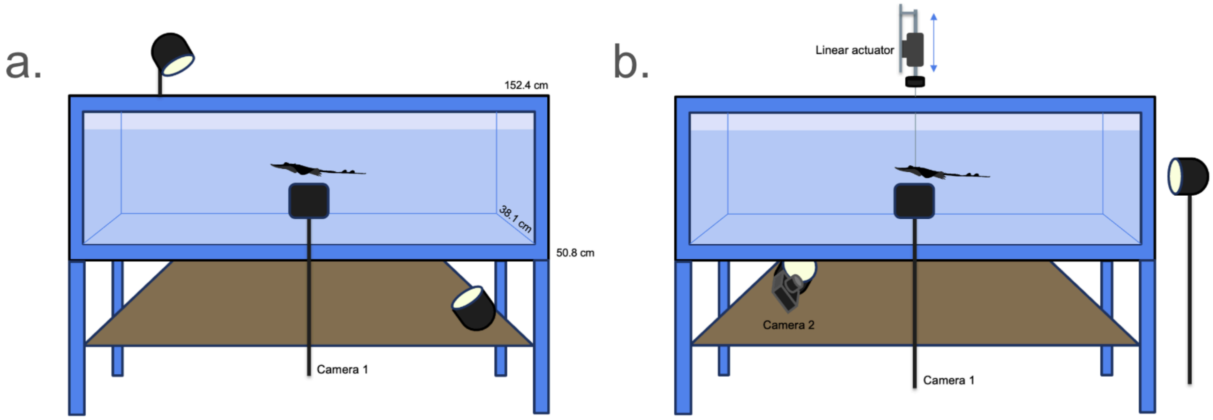

Figure 1: (a) Illustration of the flow tunnel set up for the behavioral and (b) actuation filming. During the behavioural study, there was one camera facing perpendicular to the skate with two lights facing the flow tank. In the actuation set up, there were two cameras, one lateral and the other below the flume. The lights were placed below and to the side of the flow tank. The skate was mounted onto a stick with a linear actuator. Both experiments were performed in the same flume tank.

Kinematic Analysis:

Amplitude was measured using Fiji ImageJ (Schindelin et al., 2012). Frames at maximum and minimum amplitudes were identified for each individual video (fig. 2). The known total length of the skate (184.829 mm) was used to calibrate the frames by selecting the line of full body length and setting the pixel ratio (px/mm). Once the scale was set, maximum and minimums were defined as a line measured from the tip of the wing to the midline of the skate (fig. 2). Amplitude was then calculated for each cycle ($\frac{max + min}{2}$) and averaged for each of the videos. For the live swimming videos, three consecutive flaps were used to measure amplitude for each swimming trial. For the decreased skate videos, six consecutive full flaps (after the actuator's 'warmup' cycles and during the 10 full oscillations) were used at each frequency.

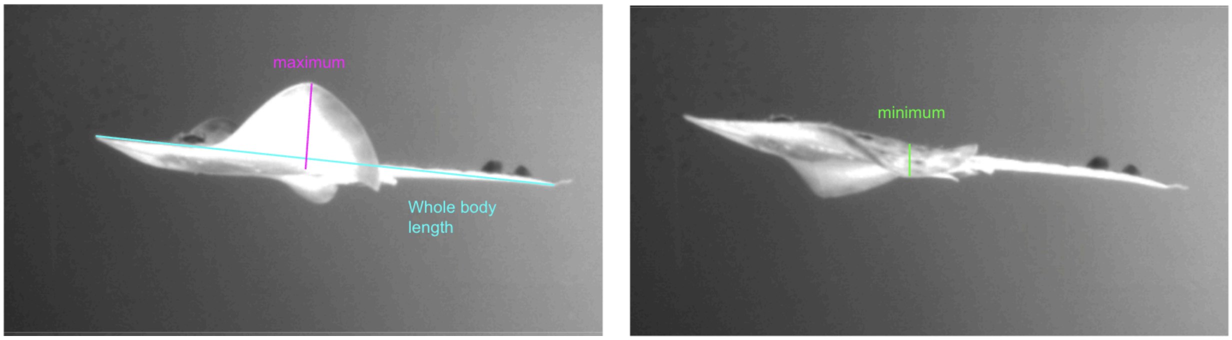

Figure 2: Whole body length was measured from the tip of the nose to the cartilaginous tip of the tail. Maximum and minimum measurements were taken from the tip of the wing to the midlateral portion of the body to calculate amplitude.

Frequency measurements were performed for the live skate videos, measured by looking at the difference in number of frames between each maximum amplitude to get one full wavelength. The frame number difference between maximum amplitudes was averaged for three full oscillations and divided by the frames per second value, 78 fps, to solve for time between each cycle. Time was then used to find frequency, (1/T) which represents the number of flaps performed per second.

For the live trials, video sections of stable swimming were used to calculate the velocity. Stable swimming was defined qualitatively by consistency of body pitch and depth. The number of flaps for each video was variable depending on how long the skate was steadily swimming. Using Fiji, the coordinates of the start and end of these phases were used to calculate distance which was divided by time based on the frame number difference (Schindelin et al., 2012). This velocity was added to the flow speed of the flume to get the total velocity of the skate.

Strouhal number was calculated ($Sr = \frac{\omega l}{v}$) for each of the swimming trials. This value is expected to fall between 0.25-0.35 for all fishes as the optimal value for trust production (Triantafyllou et al., 1993).

Wavenumber for each of the live swimming trials was calculated by averaging the wavenumbers across an entire cycle for each trial. The first selected frame was a maximum point, and nine consecutive frames were used in five frame (or 64 ms) intervals. For each frame, the fin tip was marked with points on Fiji which were converted into coordinate points (Schindelin et al., 2012). The points were then corrected onto a flat 2D plane by taking the angle of the skate and transferring all of the points. From here, each frame was fitted to a best-sine fit to get individual wavenumbers, which were then averaged for each trial (fig. 10). Nine frames were used to ensure an entire flap cycle fit into the analysis, covering a total of 40 frames.

Sine sweep testing

A calibration test was performed using a 2 cm grid to account for the diffraction of light in the water. Vinyl 2 mm black dot stickers were glued on the ventral side of the skate in the center, edges, and middle of the wing (fig. 3). The bottom camera was used to track the dots to run a point tracking displacement analysis code to calculate average gain of each point. A tracking dot was placed on the bottom of the stick the skate was mounted on to serve as the basis for input frequency. Image tracking from OpenCV within Python 3.13 was used to determine the output displacement of each point on a two-dimensional grid to calculate gain as output over input. The first frame for each frequency was then used to calculate position as real response to get wavenumber.

Figure 3: Point tracking was used to track the fin movement on the skate's ventral side with dots distributed along the entire fin and body. Stick not shown.

Computed-Tomography Scanning:

The longnose skate specimen was scanned using a Bruker Skyscan 1273 micro Computed-Tomography scanner at the Karel F. Liem Imaging Center at Friday Harbor Laboratories. The scan had a pixel spacing of 32.97 um to view the general geometry of the skate's cartilaginous skeleton including the pterygial complex and extending radials. A big skate, *Raja binoculata,* specimen from the Friday Harbor Laboratories frozen collection was dissected to take scans of the radials. The cartilage was isolated from the muscle and placed in a tube and scanned at 18.84 um. All scans were done at 65 kV and 100 uA. Images were processed using 3D Slicer (Fedorov et al., 2012).

Results:

Observational Study

Data points from the swimming videos were organized by trial to compare the amplitude, velocity, frequency, wavenumber, and Strouhal numbers. A weak positive correlation between frequency and velocity was observed with a multiple R-squared value of 0.4007 and p-value of 0.127, which is not statistically significant (fig. 4a). Between the seven swimming trails, the average frequency of the skate was 2.06 with a standard deviation of 0.06. The skate swam at an average speed of 1.24 body lengths per second with a standard deviation of 0.22 BL/s. When comparing how velocity affected strohaul there was a strong negative correlation with a multiple R-squared value of 0.6091 and p-value of 0.03839, which indicates statistical significance within a limited range (fig. 4b). There was no significant trend that related to amplitude (fig. 4 c & d) with the relationship between amplitude and Strouhal having a p-value of 0.217.

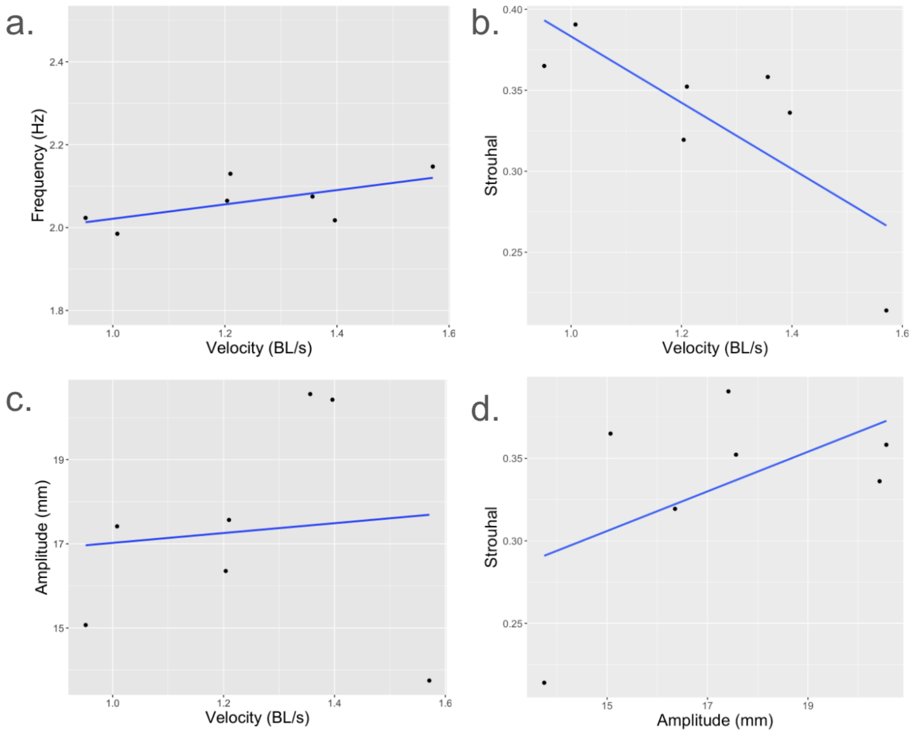

Figure 4: scatter plots of the values from the live skate video data. (a) shows a slight positive trend between frequency and velocity, (b) shows a negative trend in velocity and Strouhal number, (c) there is no discernible relationship between amplitude and velocity and (d) that as amplitude increases so does strouhal.

Computed-Tomography Scanning:

Looking at the scan of the longnose skate (fig. 5) the medial radials are catenated and more dense in contrast to the distal post-bifurcated radials. In the close up scan (fig. 6), the skate has catenated calcification, where the entirety of the radial is not calcified. Within each radial, there are three catenated spokes, two on the dorsal side and one on the ventral. Along each of the spokes, there are clear units of calcifications, or tesserae.

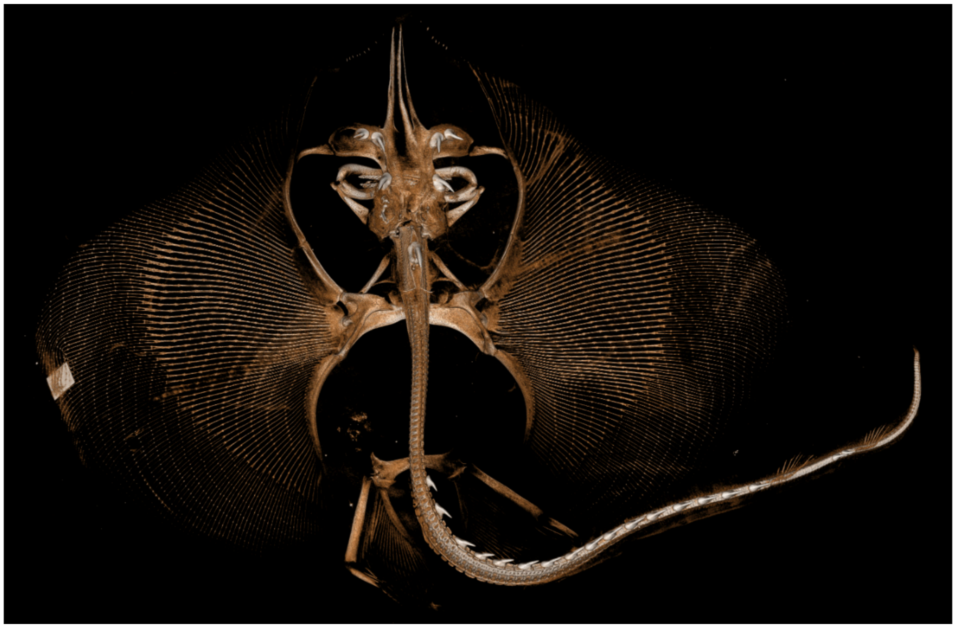

Figure 5: Superior view of computed-tomography scanned a longnose skate with a disc length of 87.mm, scanned at 32.97 um, highlighting the pelvic girdle, radials, spines, and tail of the skate. The white square on the left fin tip is a marker and not part of the skate skeleton.

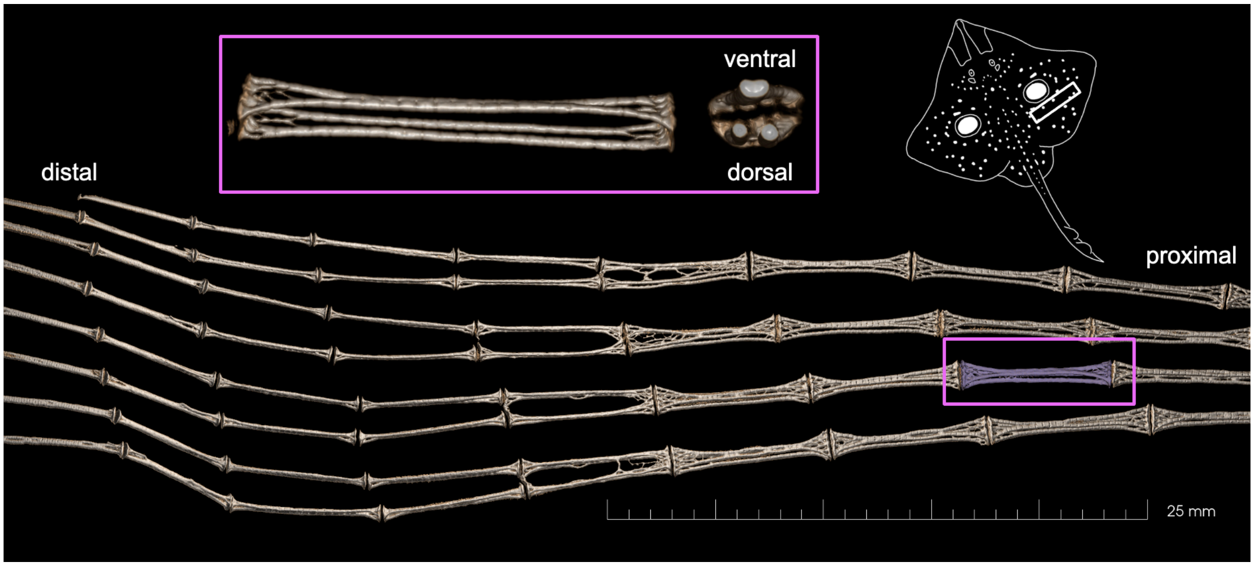

Figure. 6: Close up view of the radial structure in a big skate, with the white rectangle in the corner representing where the specimen was dissected. The radials are made up of three chains of calcification until they bifurcate.

Deceased Skate Model

Using the camera data from the side view, average amplitudes were taken for 6 oscillations at each input frequency and plotted with error bars representing one standard deviation above and below the mean (fig. 7a). From this graph, there is a significant peak at 1.9 Hz where the error bars do not overlap. From the point tracking data, a frequency response function (FRF) was made by taking input frequency over the average gain for all of the points (fig. 7b). This average gain was then plotted over frequency to get a peaked response at 2.4 Hz.

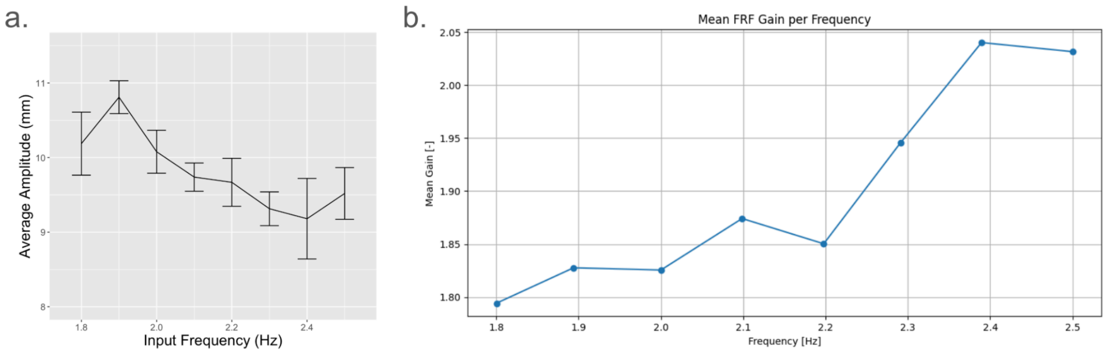

Figure 7: The frequency response functions that were (a) generated from the side-view camera (left) and (b) the bottom-view camera (right)

Gain of each individual point was analyzed by visualizing displacement by position (fig. 8). Gain was determined by looking at the input frequency of the linear actuator versus the output frequency of the individual points to get a difference in amplitude. We used only one wing's tracking points because the other wing's dots were outputting noise where dots were overlapping, and the tail points were not used because the tail is not involved with skate swimming. When calculating frequency response functions, different results were observed from the side versus bottom camera view of the deceased skate. Between figures 7 a & b, the peak response frequencies appear to be reversed, with the left graph peaking at 1.9 Hz and the right peaking at 2.4 Hz.

A standing wavenumber was calculated by taking the points from the displacement graph and collapsing them onto one y-axis (fig. 8 & 9). These points were plotted against their real response position to calculate wavenumber. Points with a greater real response correlate to the points on the tip of the fin with points lower on the axis correlating to positions more medial. These points were then fit to a best-sin-fit to get wavenumbers for all of our frequencies. In the deceased experiments, wavenumber decreased as frequency increased with a multiple R-squared 0.443 and a p-value of 0.07163 (fig. 13a) The deceased and live swimming wavenumber (fig. 10) and frequency points were graphed alongside each (fig. 13b).

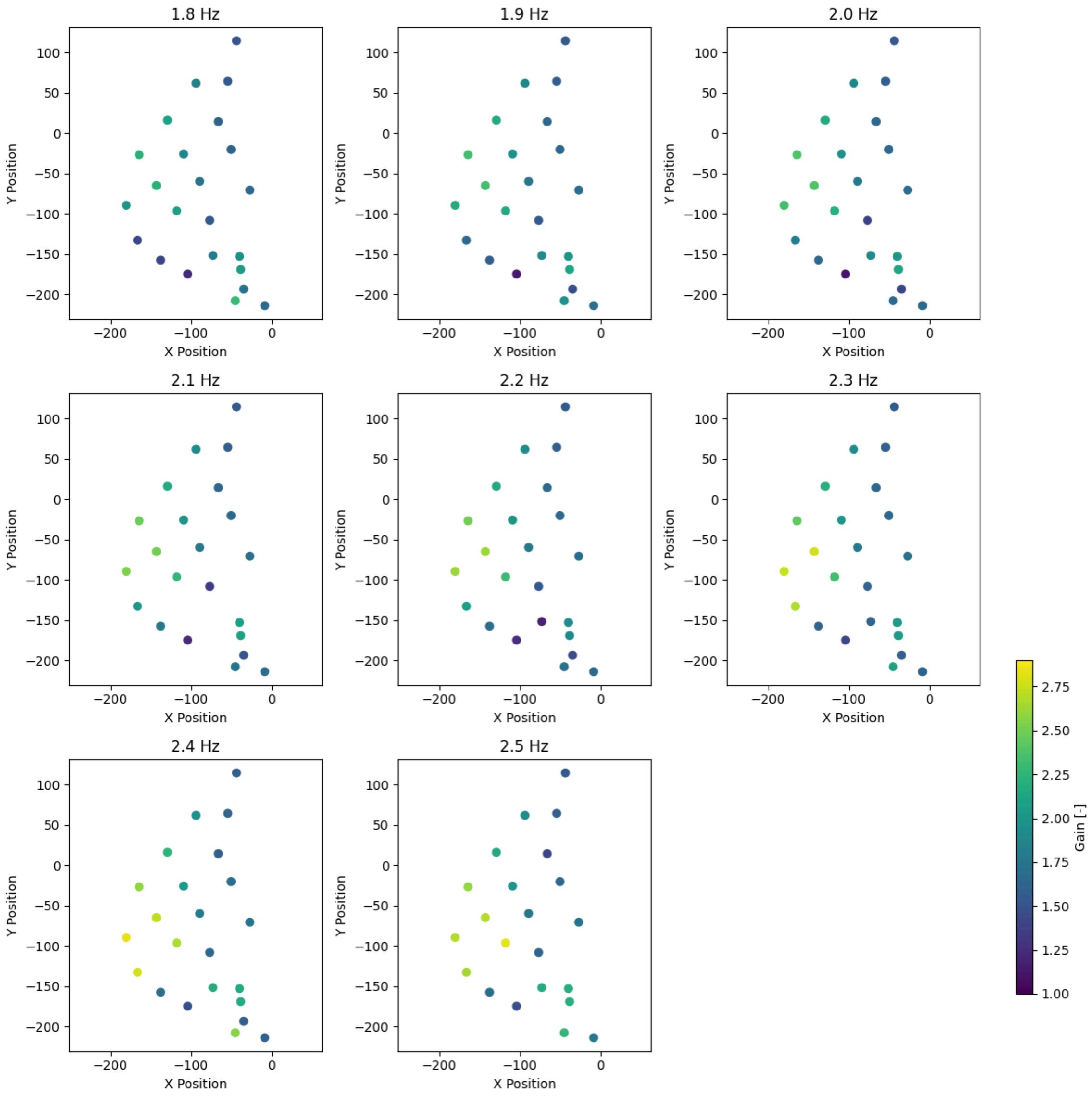

Figure 8: Shows the computed gain for each tracked point on the right fin of the skate for each sine sweep (points on ventral side). The arrangement of the dots on the graph is from the first frame, with the colors representing the maximum gain of each point throughout the entire sine sweep. Gain is defined as the displacement of the points on the z-plane (facing out of the figure), which was calculated as output of dot over input of stick. Clearly erroneous points with 0 absolute displacement were removed by filtering.

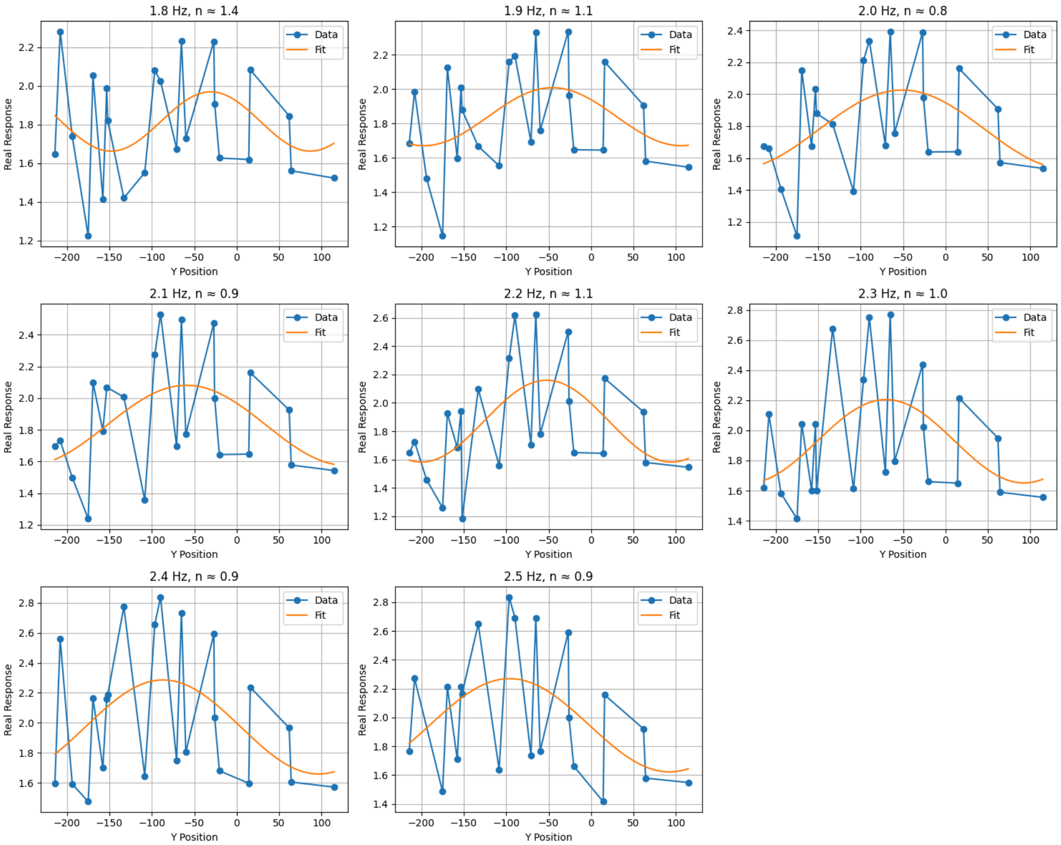

Figure 9: Shows the wavenumbers of sinusoidal fits of the points' absolute displacements for each of the frequency trials. The first frame of each trial was used to plot the y position against the real response. Y-position represents the position, posterior to anterior of the fin, with the rightmost point on the y-position representing position of the skate's nose.

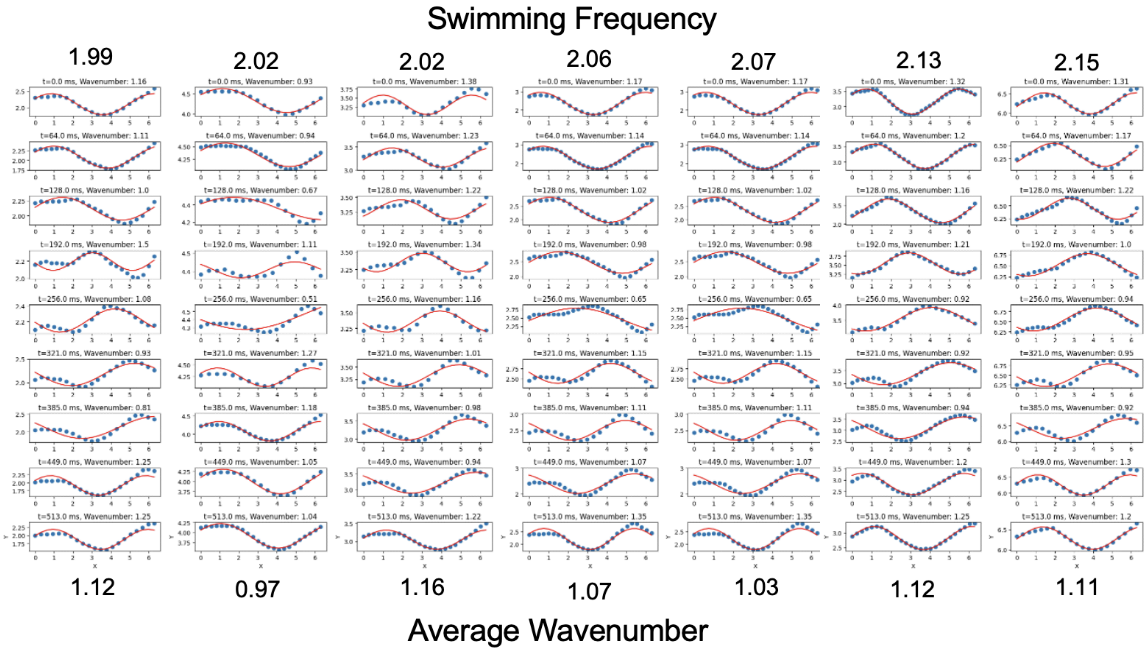

Figure 10: Wavenumber of the live skate swimming at different swimming frequencies visualized along different stages of a full flap. When adding the coordinate points in Fiji the y axis gets inverted but the wavenumber should stay the same.

Discussion

In the observational study the skate had a preferred swimming speed and frequency regardless of tank flow, suggesting that in variable conditions, the skate still has an ideal mode of swimming. The positive correlation between frequency and velocity matches literature observations between swimming speed and frequency; as flapping frequency increases, so does velocity (fig. 4a) (Rosenberger & Westneat, 1999). Small changes in frequency were able to produce larger changes in velocity, with the statistical analysis suggesting that frequency is not the only factor that skates adjust when changing their swimming speed. Within the limits of this experiment, this indicates that the skate has a preferred frequency range to swim at. The skate swam at an average speed of 1.24 body lengths per second which is within the range reported by Di Santo of a Rajadae

U-shaped metabolic speed curve, meaning the skate is swimming in a range that minimizes cost of transport (Di Santo & Kenaley, 2016).

The velocity Stouhal inverse relationship is directly predicted; velocity directly decreases Strouhal by definition. The statistical analysis shows that within this range of values, it is reasonable to conclude that increases in velocity will decrease Strouhal. This model also suggests that frequency and velocity do not increase at the same rate. Looking at fig. 4 a & b, the increase in velocity has a greater impact on Strouhal than frequency. It doesn't take a large change in frequency to increase the skate's swimming speed, which is also evident by the low range of frequencies. Variability in frequencies is present and related to velocity, but frequency does not increase to the same scale. Velocity increases at a greater rate which decreases the Strouhal denominator faster than the frequency value can make up for, further suggesting that the skate swims within an ideal range of frequencies. There is one data point that is at a much higher velocity than the others and a much lower Strouhal number. One hypothesis for this observation is that this point represents a stress response where the fish needed to generate quick motion. More data on quick response reactions would benefit our understanding of how stressors may be affecting the biomechanics of skates.

In figures 4 c & d, amplitude was not a large indicator of velocity, with Rosenberger and Wesneat suggesting that amplitude should stay constant as velocity increases (Rosenberger & Westneat, 1999). Variation of amplitude in this model may be related to another factor such as swimming directionality. Some of this variability was accounted for by using videos where the skate steadily swam but could be improved by performing more trials and increasing the number of skates used in our analysis. By definition of strouhal, as amplitude increases, so does Strouhal. This definition is loosely seen in the model (fig. 4d) but isn't statistically significant with a p-value of 0.217, suggesting that velocity and amplitude are not related. Amplitude acts on the numerator independently from velocity and hence, changes in amplitude are not strong indicators of velocity.

Looking at the skate's CT scan (fig. 5) the observed skeletal structures match the findings in Schaefer and Summers. The difference in calcification between the medial and distal radials is indicative of the fact that there is less stiffness at the tip of the wing, which is where the fin experiences the most flexure when the skate is swimming (Schaefer & Summers, 2005). The tesserae seen in figure 6 are physiologically important in distributing stress along the wing, strengthening the wing in multiple directions and allowing for greater flexibility when oscillating (Huang et al., 2017).

Comparing the modes of swimming between the deceased and live skate, it is evident that the flapping motion is an active shape that the skate is able to maintain using muscular input (fig. 11). In the behavioral trials, the maximum bend of the wing occurs as an upward flap, with the wing bending only slightly below the midline (fig. 21). When simulating the skates swimming with the deceased model, that stiffness was no longer actively controlled and the skate's fins hung down. The fins did not reach above the skate's body due to the rays negative natural buoyancy (Bone & Roberts, 1969), which outweighed the effect of the input excitation. Looking at the point tracking (fig. 8 & 9), points more distal on the body experienced greater gain which makes sense because these points represent the tips of the fin. Looking at the points in figure 9, those tip points had a greater real response correlated to maximal flexion, with points lower on the axis correlating to positions more medial and stiff. Medial points did not displace as much, meaning that the pterygial complex allows the center of the skate to remain stiff. From the behavioural trials, the amplitude peaked at 1.9 (fig. 7a) indicating a significant frequency in which the skates body likes to flap. This value is near the range of the skates preferred swimming frequency of 2.0-2.1. The ideal frequency in the dead skate was lower than the skates preferred swimming speed, which can be explained by the definition of Strouhal. Increases in stiffness will lead to an increase in natural frequency. With the live skate being less stiff, it preferred to swim at a frequency slightly higher (2.0-2.1) than the frequency we observed from the stiffening deceased skate (1.9 Hz).

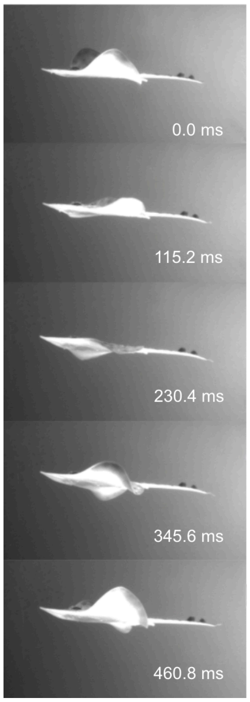

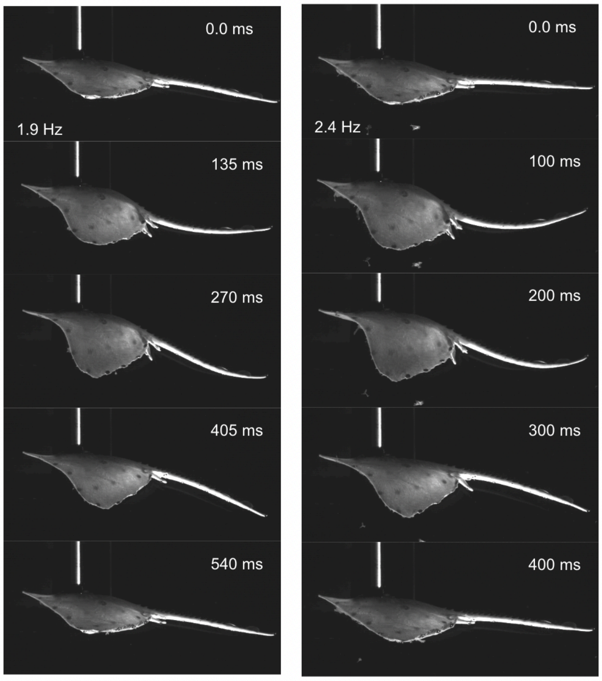

Figure 11 (left): Lateral images of the longnose skate swimming through the flume with a flow of 72.136 mm/s. The images were aligned at the skate's nose and do not show the skate moving forward. The skate swims by passing many waves down its body in an undulatory motion. Figure 12 (right): One wave cycle for the peak of 1.9 Hz and trough 2.4 Hz showing the moment where each wave hits the top peak.

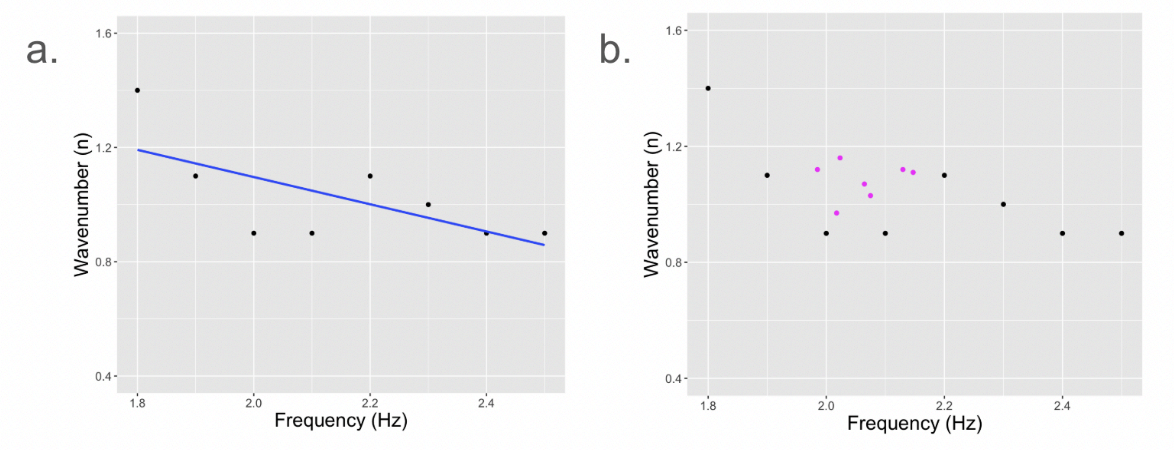

Fig 13: (a) wavenumbers for the frequency range that we excited the skate on the stick with linear best-fit line. (b) Plots the data from the deceased skate experiment (black) with the data from the swimming skate (magenta) to show that the data fall within similar ranges of each other.

The difference in FRF graphs can be explained by two factors; how gain was measured for each method, and 3D geometry. From the side, we were able to calculate the direct up-and-down displacement of the wing as a whole, whereas the bottom view looks at displacement for multiple points. The FRF generated from the bottom view took the average gain of all the points and put those points on an x-axis that represented the skate's body laterally. The FRF from the side calculated gain using the same methods as used to measure amplitude, looking at the fin tip only. The fin moved up and down in both frames and from the side view this motion was the y-axis, however from the bottom, this motion was the z-axis. This incongruity is due to the point tracking system's 2D image, it was unable to account for such large 3D displacement. When the fin moved farther up or down, the bottom camera saw that the fin was staying closer to the middle of the body. This may help explain why the peaks of each graph are inverted; from the bottom camera a greater up and down displacement appear as though the fin is staying more centered. For this study, the side calculations are a more valid calculation of amplitude (fig. 7a) staying consistent with the methods that amplitude was measured in the live swimming trials.

In the deceased experiments, wavenumber decreased as frequency increased, matching the literature expectations (Rosenberger & Westneat, 1999). Although a low multiple r-squared value is statistically significant, testing a longer range of frequencies would be redundant due to the fact that live skates swim within a fairly limited range of frequencies. The fact that the live skate swims within a consistent range of wavenumbers (fig. 13b) suggests that the animal is choosing to leverage its dynamic passivity. Rigor mortis may have also affected the results as the experiment was run approximately one hour post-mortem. The length of one cycle also changed between live swimming trails, with higher frequencies (2.15 Hz) being represented across 35 frames and lower frequencies (1.9 Hz) being 40 frames. 40 frames were used for all trials meaning that for higher frequency trials, more than one cycle is represented in the average wavenumber. This could have brought up the average for the higher frequency trials. To eliminate this potential variable we took the average wavenumber for all nine points, the first eight points, and the first seven points and compared the trends in frequency. These trials all produced the same trendline with no significant difference so this data is likely still representing the true average wavenumber at each frequency.

Based on figure 9, it is evident that a wave is present along the deceased skate's fin. Although the wave shape is different from the live skate's, a sine wave is still present. This is significant because although it was observed that lack of muscular stiffness changes the fin motion pattern, undulation is still present. These results indicate that an undullatory wave is encouraged by morphology, and that the propagation of the wave is influenced by the skeletal structure of the skate. On balance, we must conclude that morphology is a component of batoid locomotion, but muscular control is also needed to maintain posture, wave shape, and full propagation.

Looking ahead, these results suggest new ways of designing traveling wave based swimming robots by harnessing the passivity of the batoid skeletal structure. Purely-passive propulsive fins may be made more effective, while fins with sophisticated control and actuation may be made more capable. Along both of these avenues, the skeleton becomes a tuning tool for specialization.

A significant continuation of this experiment would be to investigate how skate skeletal elements might be at risk of changing climates. Di Santo investigated the development of the little skate's skeleton under changing pH and temperatures (Di Santo, 2019). Our study highlighted the importance of stiffness created by the skate's skeleton, with changes in this stiffness having the potential to increase the skate's cost of transport. We should continue to compare modes of swimming across a wider range of velocities, especially when batoids use bursts of faster swimming. According to results from Rosenberger and Westneat, frequency will continue to increase with velocity (Rosenberger & Westneat, 1999). Based on our data as well as Di Santo's velocity-metabolic data and Rosenberger's velocity-frequency graph, undullatory batoids do prefer to swim within a frequency range of around 2 Hz. Further studies should be done to see how this preferred range changes phylogenetically. Di Santo's study was on clearnose skates *Raja eglanteria* and Rosenberger looked at bluespotted ribontail rays *taeniura lymma*. More data across the batidae group would allow for a greater range of data to potentially determine what phylogenetic traits contribute to ideal frequencies of each batoid. This would allow us to cover a broader range of shapes and swimming styles to more accurately predict how these traits impact different swimming modes.

Variables

ω	Frequency
l	Amplitude
v	Velocity
Ω	Resonant frequency
k	Spring constant (stiffness)
m	Mass

Acknowledgements

This research was funded by NSF under award DBI-2149705. Special thanks to Tadd Truscott for help with python coding, Eric Loss for leading the trawling trip, and Cassandra Donatelli, Karly Cohen, and Amy Cook for organizing and supporting this REU experience.

Works Cited

Beal, D. N., Hover, F. S., Triantafyllou, M. S., Liao, J. C., & Lauder, G. V. (2006). Passive propulsion in vortex wakes. *Journal of Fluid Mechanics*, *549*, 385–402. https://doi.org/10.1017/S0022112005007925

Bone, Q., & Roberts, B. L. (1969). The density of elasmobranchs. *Journal of the Marine Biological Association of the United Kingdom*, *49*(4), 913–937. https://doi.org/10.1017/S0025315400038017

Bottom Ii, R. G., Borazjani, I., Blevins, E. L., & Lauder, G. V. (2016). Hydrodynamics of swimming in stingrays: Numerical simulations and the role of the leading-edge vortex. *Journal of Fluid Mechanics*, *788*, 407–443. https://doi.org/10.1017/jfm.2015.702

Di Santo, V. (2019). Ocean acidification and warming affect skeletal mineralization in a marine fish. *Proceedings of the Royal Society B: Biological Sciences*, *286*(1894), 20182187. https://doi.org/10.1098/rspb.2018.2187

Di Santo, V., & Kenaley, C. P. (2016). Skating by: Low energetic costs of swimming in a batoid fish. *Journal of Experimental Biology*, jeb.136358. https://doi.org/10.1242/jeb.136358

Ebert, D. A., & Compagno, L. J. V. (2007). Biodiversity and systematics of skates (Chondrichthyes: Rajiformes: Rajoidei). *Environmental Biology of Fishes*, *80*(2–3), 111–124. https://doi.org/10.1007/s10641-007-9247-0

Fedorov, A., Beichel, R., Kalpathy-Cramer, J., Finet, J., Fillion-Robin, J.-C., Pujol, S., Bauer, C., Jennings, D., Fennessy, F., Sonka, M., Buatti, J., Aylward, S., Miller, J. V., Pieper, S., & Kikinis, R. (2012). 3D Slicer as an image computing platform for the Quantitative Imaging Network. *Magnetic Resonance Imaging*, *30*(9), 1323–1341. https://doi.org/10.1016/j.mri.2012.05.001

Huang, W., Hongjamrassilp, W., Jung, J.-Y., Hastings, P. A., Lubarda, V. A., & McKittrick, J. (2017). Structure and mechanical implications of the pectoral fin skeleton in the Longnose Skate (Chondrichthyes, Batoidea). *Acta Biomaterialia*, *51*, 393–407. https://doi.org/10.1016/j.actbio.2017.01.026

Jeong, Y. D., & Lee, J. H. (2024). Hydrodynamic benefits of passive flexibility in a self-propelled oscillatory ray. *Physics of Fluids*, *36*(2), 021909. https://doi.org/10.1063/5.0179211

Koester, D. M., & Spirito, C. P. (2003). Punting: An Unusual Mode of Locomotion in the Little Skate, Leucoraja erinacea (Chondrichthyes: Rajidae). *Copeia*, *2003*(3), 553–561. https://doi.org/10.1643/CG-02-153R1

Kohannim, S., & Iwasaki, T. (2014). Analytical insights into optimality and resonance in fish swimming. *Journal of The Royal Society Interface*, *11*(92), 20131073. https://doi.org/10.1098/rsif.2013.1073

Liao, J. C., Beal, D. N., Lauder, G. V., & Triantafyllou, M. S. (2003). Fish Exploiting Vortices Decrease Muscle Activity. *Science*, *302*(5650), 1566–1569. https://doi.org/10.1126/science.1088295

Long, J. H., & Nipper, K. S. (1996). The Importance of Body Stiffness in Undulatory Propulsion. *American Zoologist*, *36*(6), 678–694. https://doi.org/10.1093/icb/36.6.678

López-Romero, F. A., Villalobos-Segura, E., Türtscher, J., Berio, F., Stumpf, S., Dearden, R. P., Kriwet, J., & Maldonado, E. (2025). Evolution of the batoidea pectoral fin skeleton: Convergence, modularity, and integration driving disparity trends. *Evolutionary Ecology*, *39*(1), 111–134. https://doi.org/10.1007/s10682-025-10330-x

Martinez, C. M., Rohlf, F. J., & Frisk, M. G. (2016). Re‐evaluation of batoid pectoral morphology reveals novel patterns of diversity among major lineages. *Journal of Morphology*, *277*(4), 482–493. https://doi.org/10.1002/jmor.20513

Rosenberger, L. J. (2001). Pectoral Fin Locomotion in Batoid Fishes: Undulation *Versus* Oscillation. *Journal of Experimental Biology*, *204*(2), 379–394. https://doi.org/10.1242/jeb.204.2.379

Rosenberger, L. J., & Westneat, M. W. (1999). Functional morphology of undulatory pectoral fin locomotion in the stingray *taeniura lymma* (Chondrichthyes: Dasyatidae). *Journal of Experimental Biology*, *202*(24), 3523–3539. https://doi.org/10.1242/jeb.202.24.3523

Schaefer, J. T., & Summers, A. P. (2005). Batoid wing skeletal structure: Novel morphologies, mechanical implications, and phylogenetic patterns. *Journal of Morphology*, *264*(3), 298–313. https://doi.org/10.1002/jmor.10331

Schindelin, J., Arganda-Carreras, I., Frise, E., Kaynig, V., Longair, M., Pietzsch, T., Preibisch, S., Rueden, C., Saalfeld, S., Schmid, B., Tinevez, J.-Y., White, D. J., Hartenstein, V., Eliceiri, K., Tomancak, P., & Cardona, A. (2012). Fiji: An open-source platform for biological-image analysis. *Nature Methods*, *9*(7), 676–682. https://doi.org/10.1038/nmeth.2019

Y Alvarado, P. V. (2011). Hydrodynamic performance of a soft body under-actuated batoid robot. *2011 IEEE International Conference on Robotics and Biomimetics*, 1712–1717. https://doi.org/10.1109/ROBIO.2011.6181536

Yang, S., Qiu, J., & Han, X. (2009). Kinematics Modeling and Experiments of Pectoral Oscillation Propulsion Robotic Fish. *Journal of Bionic Engineering*, *6*(2), 174–179. https://doi.org/10.1016/S1672-6529(08)60114-6